

The Lorenz system

James Hateley

Contents

1	Formulation	2
2	Fixed points	4
3	Attractors	4
4	Phase analysis	5
4.1	Local Stability at The Origin	5
4.2	Global Stability	6
4.2.1	$0 < \rho < 1$	6
4.2.2	$1 < \rho < \rho_h$	6
4.3	Bifurcations	6
4.3.1	Supercritical pitchfork bifurcation: $\rho = 1$	7
4.3.2	Subcritical Hopf-Bifurcation: $\rho = \rho_h$	8
4.4	Strange Attracting Sets	8
4.4.1	Homoclinic Orbits	9
4.4.2	Poincaré Map	9
4.4.3	Dynamics at ρ^*	9
4.4.4	Asymptotic Behavior	10
4.4.5	A Few Remarks	10
5	Numerical Simulations and Figures	10
5.1	Globally stable, $0 < \rho < 1$	10
5.2	Pitchfork Bifurcation, $\rho = 1$	12
5.3	Homoclinic orbit	12
5.4	Transient Chaos	12
5.5	Chaos	14
5.5.1	A plot for ρ_h	14
5.6	Other Notable Orbits	16
5.6.1	Double Periodic Orbits	16
5.6.2	Intermittent Chaos	16
5.6.3	A Periodic Orbit	18
6	MATLAB Code	18
6.1	LORENZ.m:	18
6.2	LORENZ_SYS.M	20
6.3	LORENZ_SYS_VEC.M	21
6.4	PLOTTING_SCRIPT.M	21
	Bibliography	25

1 Formulation

The Lorenz system was initially derived from a Oberbeck-Boussinesq approximation. This approximation is a coupling of the Navier-Stokes equations with thermal convection. The original problem was a 2D problem considering the thermal convection between two parallel horizontal plates. The Lorenz system arises from using a truncated Fourier-Galerkin expansion. For purposes of completeness, the system will be derived from its governing equations. The momentum equation is

$$\mathbf{u}_t + \mathbf{u} \cdot \nabla \mathbf{u} = -\frac{1}{\rho} \nabla p + \nu \bar{\Delta} \mathbf{u} + \frac{1}{\rho} \mathbf{F}$$

where p is the pressure, $\bar{\Delta}$ is the vector Laplacian, ρ is the density, ν is the kinematic viscosity and \mathbf{F} represents the external forces. In general, the continuity equation is

$$\rho_t + \nabla \cdot (\rho \mathbf{u}) = 0.$$

ρ constant reveals the incompressibility condition $\nabla \cdot \mathbf{u} = 0$. Denote the temperature of the plates by T_0 and T_1 . In this case the force $\mathbf{F} = \alpha g(T - T_0) \hat{k}$, where α is the thermal expansion constant and \hat{k} is a unit vector in the z -direction. The temperature is modeled by the equation

$$T_t + \mathbf{u} \cdot \nabla T = \kappa \Delta T$$

with κ being the diffusivity constant. Converting to the dimensionless equations:

$$\begin{aligned} \mathbf{u}_t + \mathbf{u} \cdot \nabla \mathbf{u} &= -\nabla p + \sigma \bar{\Delta} \mathbf{u} + r \sigma \phi \hat{k} \\ \nabla \cdot \mathbf{u} &= 0 \\ \phi_t + \mathbf{u} \cdot \nabla \phi &= v_3 + \Delta \phi \end{aligned}$$

where σ is the Prandtl number, r is the Rayleigh number, \mathbf{v} is the velocity given component-wise by v_i . Using the stream function; $\psi(y, z, t)$, formulation with $v_1 = 0$,

$$v_2 = \frac{\partial \psi}{\partial z}, \quad v_3 = -\frac{\partial \psi}{\partial y}$$

the incompressibility condition, $\nabla \cdot \mathbf{u} = 0$, is satisfied. As the problem is set up, the only nonzero component of the vorticity is in the x -direction, call this ξ

$$\xi = \frac{\partial v_3}{\partial y} - \frac{\partial v_2}{\partial x} = -\Delta \psi$$

Taking curl of the momentum equation and projecting in the x -direction, the pressure p vanishes from the equation and we have the equation for the vorticity ξ .

$$\xi_t + \mathbf{u} \cdot \nabla \xi = \sigma \Delta \xi + r \sigma \phi_y$$

By using the chain rule we can write the system:

$$\begin{aligned} \xi_t + \left| \frac{\partial(\xi, \psi)}{\partial(y, z)} \right| &= \sigma \Delta \xi + r \sigma \phi_y \\ \phi_t + \left| \frac{\partial(\xi, \psi)}{\partial(y, z)} \right| &= \Delta \phi - \psi_y \\ \xi &= -\Delta \psi \end{aligned}$$

Note that $\left| \frac{\partial(\xi, \psi)}{\partial(y, z)} \right|$ is just the Jacobian of (ξ, ψ) with respect to (y, z) . Now consider the Fourier-Galerkin expansion in complex form:

$$\begin{aligned} \psi(y, z, t) &= \sum_{m, n \in \mathbb{Z}} a_{n, m} \exp(im\pi z) \exp(im\pi y) \\ \phi(y, z, t) &= \sum_{m, n \in \mathbb{Z}} b_{n, m} \exp(im\pi z) \exp(im\pi y) \end{aligned}$$

A single term expansion for the stream function is,

$$\psi(y, z, t) = a(t) \sin(\pi z) \sin(k\pi y)$$

where $a(t)$ represents convection rolls with wave number k in the y -direction. A two term expansion for the temperature is

$$\phi(y, z, t) = b(t) \sin(\pi z) \cos(k\pi y) + c(t) \sin(2\pi z)$$

where $b(t)$ represents convection rolls with wave number k in the y -direction and $c(t)$ approximates the mean temperature profile due to convection. The Jacobians are given by

$$\begin{aligned} \left| \frac{\partial(\xi, \psi)}{\partial(y, z)} \right| &= \frac{k\pi^4}{4} a^2(t) (1 + k^2) \left(\sin(2\pi z) \sin(2k\pi y) - \sin(2\pi z) \sin(2k\pi y) \right) \\ \left| \frac{\partial(\phi, \psi)}{\partial(y, z)} \right| &= -\frac{k\pi^2}{4} a(t)b(t) \left(\sin(2\pi z) \sin^2(2k\pi y) - \sin(2\pi z) \cos^2(k\pi y) \right) \\ &\quad - 2k\pi^2 a(t)c(t) (\sin(\pi z) \cos(2\pi z) \cos(k\pi y)) \end{aligned}$$

If the projection of the error on the Fourier basis functions is zero the residual error in the truncation is minimized. Multiplying the equation for the vorticity by $\sin(\pi z) \sin(k\pi y)$ and integrating in z from 0 to 1; the distance between the two plates, and integrating in y from 0 to $2/k$ gives:

$$a_t = -\sigma\pi(1 + k^2)a(t) - \frac{k\pi}{\pi(1 + k^2)} \sigma r b(t).$$

Multiplying equation for the temperature by $\sin(\pi z) \sin(k\pi y)$ and integrating in z from 0 to 1, the distance between the two plates and integrating in y from 0 to $2/k$ reveals:

$$\begin{aligned} b_t + k\pi^2 a(t)c(t) &= -\pi(1 + k^2)b(t) - k\pi a(t) \\ c_t - \frac{\pi^2}{k} a(t)b(t) &= -\pi^2 c(t) \end{aligned}$$

rescaling the equation as $\tau = \pi^2(1 + k^2)t$ and defining

$$\hat{b}(\tau) = -\frac{\sigma b(t)}{\pi^3(1 + k^2)^2}, \quad \hat{c}(\tau) = -\frac{k^2 r c(t)}{\pi^3(1 + k^2)^3}$$

we arrive at the system:

$$\begin{aligned} \frac{da}{d\tau} &= -\sigma a(\tau) + \sigma \hat{b}(\tau) \\ \frac{db}{d\tau} &= -\hat{b}(\tau) + \frac{k^2 r}{\pi^4(1 + k^2)^3} a(\tau) \\ \frac{dc}{d\tau} &= -\frac{k}{1 + k^2} c(\tau) + \frac{k^2}{2(1 + k^2)^2} a \hat{b} \tau \end{aligned}$$

Rescaling once more, define,

$$X(\tau) = \frac{k}{\sqrt{2}(1 + k^2)} a(\tau), \quad Y(\tau) = \frac{k}{\sqrt{2}(1 + k^2)} \hat{b}(\tau), \quad Z(\tau) = \hat{c}(\tau)$$

We arrive at the the Lorenz system:

$$\begin{cases} \frac{dX}{d\tau} = \sigma(Y - X) \\ \frac{dY}{d\tau} = -Y + \rho X - XZ, & \rho = \frac{k^2 r}{\pi^4(1 + k^2)^3} \\ \frac{dZ}{d\tau} = -\beta Z + XY, & \beta = \frac{4}{1 + k^2} \end{cases}$$

where σ is the Prandtl number, ρ is the a rescaling of the Rayleigh number and β is an aspect ratio.

2 Fixed points

For the remainder of this paper, the dot notation will be used to denote the derivative with respect to time, the system is then written as

$$\begin{cases} \dot{x} = \sigma(y - x) \\ \dot{y} = \rho x - y - xz \\ \dot{z} = -\beta z + xy \end{cases} \quad . \text{ If } \mathbf{x} = \begin{pmatrix} x \\ y \\ z \end{pmatrix} \text{ and } \mathbf{F} = \begin{pmatrix} \sigma(y - x) \\ \rho x - y - xz \\ -\beta z + xy \end{pmatrix},$$

in vector form the system becomes $\dot{\mathbf{x}} = \mathbf{F}$. The fixed points are given by $\mathbf{F} = 0$, solving this system reveals that the fixed points are

$$p = (0, 0, 0), \quad q_{\pm} = (\pm\sqrt{\beta(\rho - 1)}, \pm\sqrt{\beta(\rho - 1)}, \rho - 1).$$

Denote the space of parameters by $\Lambda = (\rho, \sigma, \beta)$, for $\rho, \sigma, \beta > 0$.

3 Attractors

Computing the flow of the vector field \mathbf{F} ,

$$\nabla \cdot \langle \dot{x}, \dot{y}, \dot{z} \rangle = \nabla \cdot \mathbf{F} = -(\sigma + 1 + \beta) < 0$$

Consider a closed surface in the phase space, say $S(t)$, with volume $V(t)$. Then

$$\dot{V}(t) = \int_{S(t)} \mathbf{F} \cdot ds = \int_{V(t)} \nabla \cdot \mathbf{F} dV = -(\sigma + 1 + \beta)V(t)$$

and so

$$V(t) = \exp(-(\sigma + 1 + \beta)t)V(0).$$

Hence volumes in phase space shrink exponentially fast to a set of measure zero. This means that given a set of initial conditions with positive measure, the all trajectories will converge to a set of measure zero. So there is some attracting set for any set of parameters $\gamma \subset \Lambda$.

Now consider the function $v(\mathbf{x})$ defined by

$$v(\mathbf{x}) = \rho x^2 + \sigma y^2 + \sigma(z - 2r)^2.$$

Clearly $v(\mathbf{x}) \geq 0$ and $v(\mathbf{x}) = 0$ at p . Computing the derivative $v(\dot{\mathbf{x}}(t))$ and plugging in \mathbf{F} ,

$$\begin{aligned} v(\dot{\mathbf{x}}(t)) &= 2\rho x\dot{x} + 2\sigma y\dot{y} + 2\sigma(z - 2r)\dot{z} \\ &= -\sigma(\rho x^2 + y^2 + \beta z^2 - 2\beta\rho z). \end{aligned}$$

Define \mathcal{R} as the region where $v(\dot{\mathbf{x}}(t)) > 0$, i.e.,

$$\mathcal{R} = \{(x, y, z) : \rho x^2 + y^2 + \beta z^2 < 2\beta\rho z\}$$

The boundary of this region as an ellipsoid,

$$\partial\mathcal{R} = \{(x, y, z) : \rho x^2 + y^2 + \beta z^2 = 2\beta\rho z\}.$$

Now define the region \mathcal{S} as,

$$\mathcal{S} = \{(x, y, z) : x^2 + y^2 + (z - \rho - \sigma)^2 = r^2\}.$$

Choose r large enough such that \mathcal{R} is contained inside a region bounded by the surface \mathcal{S} . Now if a point \mathbf{x}_0 lies outside of \mathcal{S} , then it also lies outside of \mathcal{R} . Hence $v(\mathbf{x}_0) < 0$. Then starting at \mathbf{x}_0 , $v(\mathbf{x})$ decreases with time and within finite time enters \mathcal{S} . Also, we have that $v(\mathcal{S}) \leq 0$, so once a trajectory crosses \mathcal{S} it cannot leave it. So for any parameters in Λ , any phase portrait will be bounded.

4 Phase analysis

The linearization is given by the matrix

$$A(x, y, z) = \frac{\partial(\dot{x}, \dot{y}, \dot{z})}{\partial(x, y, z)} = \begin{bmatrix} -\sigma & \sigma & 0 \\ -\rho - z & -1 & -x \\ y & x & -\beta \end{bmatrix}.$$

As the eigenvalues are given by the characteristic equation, which is

$$c_A(\lambda) = -\lambda^3 + \text{tr}(A)\lambda^2 - \frac{1}{2}(\text{tr}(A^2) - \text{tr}^2(A))\lambda + \det(A).$$

The needed components are computed to be:

$$\begin{aligned} \det(A) &= \rho\beta(s - z - 1) - sx(x + y) \\ \text{tr}(A) &= -(\sigma + 1 + \beta) \\ \text{tr}(A^2) &= 2\sigma(\rho - z) - 2x^2 + \beta^2 + 1 + \sigma^2. \end{aligned}$$

4.1 Local Stability at The Origin

Computing the roots of the characteristic equation $A(p)$, the eigenvalues are

$$\lambda_1 = -\beta, \quad \lambda_{\pm} = \frac{1}{2}(-1 - \sigma \pm \sqrt{\mathcal{D}})$$

where \mathcal{D} is given by;

$$\mathcal{D} = 4\rho\sigma + \sigma^2 - 2\sigma + 1.$$

The discriminant for the characteristic equation is actually a fourth order polynomial in terms of σ . As β does not appear in λ_{\pm} , the dynamics near the origin for the eigenspaces of λ_{\pm} for the linearization are independent of the parameter β . Solving \mathcal{D} for σ ,

$$\sigma_{\pm} = -2\rho + 1 \pm 2\sqrt{\rho^2 - \rho}.$$

The other root to the discriminant of the characteristic equation, has an algebraic multiplicity of two and is,

$$\sigma_1 = \frac{\beta(\beta - 1)}{\beta + \rho - 1}.$$

As $\rho > 0$, we have 3 cases to analyze; $0 < \rho < 1$, $\rho = 1$ and $1 < \rho$. As $0 < \sigma$ and $\sigma_{\pm} < 0$, since \mathcal{D} is always positive.

For $0 < \rho < 1$, all eigenvalues are negative, so locally the origin is a sink. At $\rho = 1$, the eigenvalues are $0, -(1 + \sigma), -\beta$. As zero is an eigenvalue, more work needs to be done to determine local stability. For $1 < \rho$,

$$-1 - \sigma - \sqrt{\mathcal{D}} < 0 < -1 - \sigma + \sqrt{\mathcal{D}},$$

and so the origin is a saddle node. Computing the Eigenvectors;

$$E_1 = \begin{pmatrix} 0 \\ 0 \\ 1 \end{pmatrix}, \quad E_{\pm} = \begin{pmatrix} \frac{2s}{s - 1 \pm \sqrt{4ps + s^2 - 2s + 1}} \\ 1 \\ 0 \end{pmatrix}.$$

Where E_1 , and E_{\pm} correspond to λ_1 , and λ_{\pm} respectively. Except for $\rho = 1$, the Eigenvectors for the linearization will be tangential to the trajectory close to the origin. So E_1 is always a stable manifold for all values of (σ, ρ, β) . For $p < 1$, both E_{\pm} are stable. For $p > 1$, E_- is a stable, while E_+ is unstable.

4.2 Global Stability

In this section we consider the global behavior of the system for values of $\rho \neq 1$, $0 < \rho < \rho_h$, where ρ_h will be determined later.

4.2.1 $0 < \rho < 1$

Consider the potential function

$$V(x, y, z) = \frac{x^2}{\sigma} + y^2 + z^2 \geq 0.$$

Computing $\dot{V}(\mathbf{x})$,

$$\begin{aligned} \dot{V}(x(t), y(t), z(t)) &= \frac{2x\dot{x}}{\sigma} + 2y\dot{y} + 2z\dot{z} \\ &= 2(\rho + 1)xy - x^2 - y^2 - \beta z^2 \\ &= -2\left(x - \frac{\rho + 1}{2}y\right)^2 - 2\left(1 - \left(\frac{\rho + 1}{2}\right)y\right)y^2 - 2\beta z^2. \end{aligned}$$

So when $0 < \rho < 1$, we have $1 - (\frac{\rho+1}{2}) > 0$, so the potential function is strictly decreasing for values away from p . Hence as $t \rightarrow \infty$, $V(t) \rightarrow 0$ so $(x(t), y(t), z(t)) \rightarrow p$. Thus the origin is a global attractor for $0 < \rho < 1$.

4.2.2 $1 < \rho < \rho_h$

First observe the system is symmetric in (x, y) , i.e. if $(x(t), y(t), z(t))$ is a solution, then $(-x(t), -y(t), z(t))$ is a solution as well. The fixed points

$$q_{\pm} = (\pm\sqrt{\beta(\rho - 1)}, \pm\sqrt{\beta(\rho - 1)}, \rho - 1).$$

only exist for $\rho > 1$. Because of the symmetry, it suffices to only consider one of them, say q_+ . The characteristic equation is

$$c_{A(q_{\pm})}(\lambda) = \lambda^3 + (\beta + \sigma + 1)\lambda^2 + \beta(\sigma + \rho)\lambda + 2\beta\sigma(\rho - 1).$$

So we have the following quantities:

$$\begin{aligned} \det(A(q_+)) &= 2\beta\sigma(\rho - 1) \\ \text{tr}(A(q_+)) &= -(\sigma + 1 + \beta) \\ \text{tr}(A(q_+)^2) &= -2\beta(\sigma + \rho) - (\sigma + 1 + \beta). \end{aligned}$$

In general the discriminant of a cubic characteristic equation is given by:

$$\mathcal{D} = 9(\text{tr}(A))(\text{tr}(A^2) - \text{tr}^2(A)) \det(A) - 4 \text{tr}^3(A) \det(A) + \frac{1}{4} \text{tr}^2(A)(\text{tr}(A^2) - \text{tr}^2(A))^2 - \frac{1}{2}(\text{tr}(A^2) - \text{tr}^2(A)) - 27 \det(A)^2.$$

Where if $\mathcal{D} > 0$, there are three distinct real roots, $\mathcal{D} = 0$, there is a multiple root and all its roots are real. If $\mathcal{D} < 0$, there is one real root and two complex conjugate roots. As this is a horrid expression, it will be skipped. The value of ρ_h will be determined by easier means in section 4.3.2. Following the text; if $\sigma - 1 \leq \beta$, then the linearization for q_{\pm} are stable. Conversely if $\sigma > 1 + \beta$, then the linearization for q_{\pm} are stable for

$$1 < \rho < \rho_h.$$

4.3 Bifurcations

In this section, the two values of $\rho = 1$ and $\rho = \rho_h$ are analyzed. Let $\gamma \in \Lambda$ and denote $\dot{\mathbf{x}} = \phi(\mathbf{x}, \gamma)$, as a one-parameter family. Necessary conditions for a bifurcation at a point $p \in \mathbb{R}^3$ and a $\gamma_0 \in \Lambda$ are given by;

$$D_{\mathbf{x}}\phi(p, 0) = 0, \quad \phi(p, \gamma_0) = 0.$$

4.3.1 Supercritical pitchfork bifurcation: $\rho = 1$

First we have $\det(A(p)) = \beta\sigma(\rho - 1)$, and so a bifurcation point is at $\rho = 1$. As $\rho < 1$ to $\rho > 1$, the phase portrait gains two fixed points, while the origin goes from stable to unstable. It is easy to see that $D_{\mathbf{x}}\phi(p, 0) = \phi(0, 1) = 0$, and local symmetry $D_{\mathbf{x}}^2\phi(p, 0) = 0$. This is a pitchfork bifurcation.

In order to determine what type of pitchfork bifurcation this is, we need to extend the system. Introducing a new parameter, $r = \rho - 1$, we find

$$\dot{y} = (r + 1)x - y - xz.$$

The linearization and the eigenvalues remain the same. Previously the eigenvalues are computed to be $\lambda_i = 0, -(\sigma + 1), -\beta$. Simplifying the eigenvectors computed above and writing them in a matrix T ;

$$T = \begin{pmatrix} 1 & \sigma & 0 \\ 1 & -1 & 0 \\ 0 & 0 & 1 \end{pmatrix}.$$

Where they are ordered by $\lambda_i = 0, -(\sigma + 1), -\beta$, for $i = 1, 2, 3$. Denote $D = \text{diag}(\lambda_i)$, a diagonal matrix with the eigenvalues in the diagonal, i.e. $T^{-1}A(p)T = D$. Let $\mathbf{u} = (u, v, w)$, rewriting the system as $\mathbf{F}(\mathbf{u})$ with the linearization,

$$\mathbf{F}(\mathbf{u}) = D\mathbf{u} + T^{-1}R(T\mathbf{u}),$$

where $R(\mathbf{x}) = F(\mathbf{x}) - A(p)\mathbf{x}$. Computing,

$$R(T\mathbf{u}) = \begin{pmatrix} 0 \\ (r-w)(sv-u) \\ (sv+u)(u-v) \end{pmatrix}, \quad T^{-1}R(T\mathbf{u}) = \begin{pmatrix} \frac{\sigma}{1+\sigma}(r-w)(u+\sigma v) \\ -\frac{1}{1+\sigma}(r-w)(u+\sigma v) \\ (u+\sigma v)(u-v) \end{pmatrix}.$$

Thus the extended system becomes;

$$\begin{cases} \dot{u} = \frac{\sigma}{1+\sigma}(r-w)(u+\sigma v) \\ \dot{v} = -(1+\sigma)v - \frac{1}{1+\sigma}(r-w)(u+\sigma v) \\ \dot{w} = -\beta w + (u+\sigma v)(u-v) \\ \dot{r} = 0 \end{cases}.$$

The center manifold will be of the form

$$W^c = \{(u, v, w, r) : v = h_1(u, r), w = h_2(u, r), h_i(0, 0) = 0, Dh_i(0, 0) = 0\}.$$

Writing the power series for h_i up to quadratic terms,

$$\begin{aligned} h_1(u, r) &= a_0 + a_{0,1}u + a_{1,0}r + a_{2,0}u^2 + a_{1,1}ur + a_{0,2}r^2 + \mathcal{O}(3) \\ h_2(u, r) &= b_0 + b_{0,1}u + b_{1,0}r + b_{2,0}u^2 + b_{1,1}ur + b_{0,2}r^2 + \mathcal{O}(3) \end{aligned}$$

Applying the conditions $h_i(0, 0) = 0, Dh_i(0, 0) = 0$ and truncating the series;

$$\begin{aligned} h_1(u, r) &= a_{2,0}u^2 + a_{1,1}ur + a_{0,2}r^2 \\ h_2(u, r) &= b_{2,0}u^2 + b_{1,1}ur + b_{0,2}r^2 \end{aligned}$$

Taking derivative with respect to t and using that $\dot{r} = 0$;

$$\begin{aligned} \dot{h}_1(u, r) &= 2a_{2,0}u\dot{u} + a_{1,1}\dot{u}r, \\ \dot{h}_2(u, r) &= 2b_{2,0}u\dot{u} + b_{1,1}\dot{u}r. \end{aligned}$$

Substituting in these values for v and w and matching coefficients reveals,

$$a_{2,0} = a_{1,1} = a_{0,2} = b_{1,1} = b_{0,2} = 0, \quad b_{2,0} = \frac{1}{\beta}$$

What remains is:

$$\dot{u} = \frac{\sigma}{1 + \sigma} \left(ru - \frac{u^3}{\beta} \right), \quad \dot{r} = 0$$

The equilibrium is stable for $r \leq 0$ and unstable for $r > 0$, which affirms the previous results of $\rho \leq 1$ and $\rho > 1$, respectively. The sign in front of the cubic term is negative, which is a supercritical pitchfork bifurcation.

4.3.2 Subcritical Hopf-Bifurcation: $\rho = \rho_h$

A Hopf bifurcation occurs when a pair of complex conjugate eigenvalues cross the imaginary axis. This means as $\rho < \rho_h$ goes to $\rho > \rho_h$, the real parts of the eigenvalues vanish at $\rho = \rho_h$. The characteristic equation at q_{\pm} was computed earlier to be;

$$c_{A(q_{\pm})}(\lambda) = \lambda^3 + (\beta + \sigma + 1)\lambda^2 + \beta(\sigma + \rho)\lambda + 2\beta\sigma(\rho - 1)$$

Plugging in for ρ_h and solving the eigenvalues are obtained,

$$\lambda_1 = -(\beta + \sigma + 1), \quad \lambda_{\pm} = \pm i \sqrt{\frac{2\sigma(\sigma + 1)}{\sigma - \beta - 1}}$$

This is a Hopf bifurcation. The value for ρ_h can easily be determined considering purely imaginary roots. Let $\lambda = i\mu$, for $\mu \in \mathbb{R}$, plugging this back into the characteristic equation,

$$c_{A(q_{\pm})}(i\mu) = -i\mu^3 - (\beta + \sigma + 1)\mu^2 + i\beta(\sigma + \rho)\mu + 2\beta\sigma(\rho - 1) = 0$$

Taking real and imaginary parts, reveals that

$$\mu^2 = \frac{2\sigma\beta(\rho - 1)}{\sigma + \beta + 1}, \quad \mu^3 = \mu\beta(\sigma + \rho)$$

As $\mu \neq 0$, equating the two expressions and solving for ρ , ρ_h is found to be

$$\rho_h = \frac{\sigma(\sigma + \beta + 3)}{\sigma - \beta - 1}$$

As the eigenvectors are an eye sore, they will be omitted. Instead, notice that if $\rho > 1$, the characteristic equation $c_{A(q_{\pm})}(\lambda)$ has only positive coefficients. As the origin is unstable. We can conclude, from the elementary symmetric polynomials, that if the roots are real they must be negative. So the points q_{\pm} are stable for the eigenvalues are real. This affirms what is said in section 4.2.2. Upon some horrible omitted calculations, for $\rho_h < \rho$, the two critical points q_{\pm} have a two dimensional unstable manifold and a one dimensional stable manifold. At $\rho = \rho_h$, there is a two dimensional center manifold. The algebra for this is a nightmare, but upon doing this, we have that for $\sigma > \beta + 1$ the bifurcation is subcritical. The stable points for q_{\pm} lose their stability by absorbing an unstable periodic orbit. This phenomena is the subject of the next section, the origin of these periodic orbits.

4.4 Strange Attracting Sets

A strange attractor is a region in space that is invariant under the evolution of time and attracts most trajectories and has a high sensitivity to initial conditions. For $1 < \rho$, there is a stable manifold containing p which divides integral curves. These curves spiral towards q_{\pm} . As ρ approaches ρ_h , the trajectories become larger spirals. As $\rho > \rho_h$, trajectories on one side of the stable manifold of the origin cross over and start spiraling towards the other side.

4.4.1 Homoclinic Orbits

If a trajectory $\phi(\mathbf{x}, \gamma^*)$ starts at a point \mathbf{x}_0 , not on the stable manifold, and reaches \mathbf{x}_1 in a certain time t_1 , one would expect that for a small enough perturbation of the initial condition that $\phi(\mathbf{x}, \gamma^*)$ starting at $\mathbf{x}_0 \pm \epsilon$ would reach a neighborhood of \mathbf{x}_1 at the same time t_1 . As the stable manifold includes the z-axis, perturbing off of it will send a trajectory towards q_{\pm} depending on the direction of the perturbation. What is unexpected is that a small perturbation in the parametric space, $\phi(\mathbf{x}, \gamma^* \pm \delta)$, for specific values of γ^* will cause the trajectory to flow towards another fixed point. For example,

$$\phi(\mathbf{x}, (\rho^*, \sigma, \beta)) \rightarrow q_+, \quad \text{while} \quad \phi(\mathbf{x}, (\rho^* + \delta, \sigma, \beta)) \rightarrow q_-$$

The change in direction after such a small change in the parameter space can be explained by a homoclinic orbit. Because of the sensitivity to round off error, and the limit of machine precision, these orbits are hard to compute numerically. However, they can be observed numerically with small perturbations in the parametric space. Because of this, one might expect a homoclinic bifurcation to occur. To my knowledge there is no analytical proof for when homoclinic orbits appear, in general. Proof for specific cases are given in [2, 3].

4.4.2 Poincaré Map

We can deduce the existence of a homoclinic orbit from the the Poincaré map. Suppose for a range of parameters we can construct the following surface. Let \mathcal{S} be a surface that contains the fixed points q_{\pm} and their stable manifold such that \mathcal{S} intersects the 2D stable manifold at the origin along some curve $c(t)$. Also choose \mathcal{S} such that any trajectory starting in \mathcal{S} returns to \mathcal{S} . This defines a Poincaré Map, on $\mathcal{S} \setminus c(t)$. Now denote $F = P(\mathcal{S}) \cap \mathcal{S}$ as the return map. First, the curve $c(t)$ is mapped to two point by F , call these c_{\pm} . By construction, c_{\pm} are where the unstable manifold of the origin hits \mathcal{S} for the first time. Now fixing a coordinate system on \mathcal{S} , say (u, v) , and let $u = 0$ define the curve $c(t)$. Write F as,

$$F(u, v) = (f(u), g(u, v))$$

Now if the return map F can be filled by a continuum of arcs, such that each arc is taken by the return map to another arc, then this is a contracting foliation. Assuming this ([4] Ch. 3), $0 < g_v(u, v) < 1$ for $u \neq 0$ a $g \rightarrow 0$ and $u \rightarrow 0$. We want to observe the behavior of the solution as ρ increase to ρ^* and beyond, for some values ρ^* .

4.4.3 Dynamics at ρ^*

Results from references are summarized. As $\rho = \rho^*$ the intersection of the unstable manifold of the origin with the return map hits c_{\pm} , this implies that the unstable manifold of the origin is contained in the stable manifold, so a homoclinic orbit appears.

For $\rho > \rho^*$, numerical evidence shows the following. The return map, F has two new fixed points. These points are from the limit cycles which arise at ρ^* from the homoclinic orbits. There exists an Cantor-like invariant set Ω between these fixed points, this is what some call a strange invariant set. Points that enter Ω stay forever within this region. Furthermore, the dynamics on this set are conjugate to the shift map, s , of two symbols, [4, 6]

$$s(w) = w_2 w_3 w_4 \dots, \quad w = w_1 w_2 w_2 \dots, \quad w \in \{0, 1\}.$$

The set of all periodic sequences in Ω is countable and dense in Ω . Suppose that all non-periodic orbits in Ω can be enumerated as well. Using a cantor diagonal argument, we can construct a sequence with w_1 different than in the first sequence, w_2 different from the second sequence and so forth. Thus, the set of all non-periodic orbits must be uncountable. So there exists, within Ω , a countable number of periodic orbits and an uncountable infinity of aperiodic orbits and orbits that tend to the origin.

On this set Ω , the dynamics also show extreme sensitive dependence on initial data. There are two possible conclusions that arise from the appearance of this set Ω . First, the two simplest periodic orbits are likely the

periodic orbits for which the subcritical Hopf bifurcation at ρ_h absorbs. Since other periodic orbits cannot be considered as the z-axis is invariant, an orbit which winds around the axis will never be able to separate itself from it, since it cannot cross it. Second, as the system is always bounded, this invariant set must be the attractor after the three critical points become unstable.

4.4.4 Asymptotic Behavior

The chaos vanishes for ρ large enough. Let $\epsilon = \rho^{-1/2}$, and consider the scaling

$$x = u/\epsilon, \quad y = v/(\epsilon^2\sigma), \quad z = (w/\sigma + 1)/\epsilon^2, \quad t = \epsilon\tau.$$

With this scaling the system becomes;

$$\begin{cases} \dot{u} = v - \sigma\epsilon u \\ \dot{v} = -uw - \epsilon v \\ \dot{w} = uw - \beta\epsilon(w + \sigma) \end{cases} .$$

Looking at the leading order terms

$$\begin{cases} \dot{u} = v \\ \dot{v} = -uw \\ \dot{w} = uw \end{cases} .$$

this lead to a pair of integral curves

$$u^2 - 2v = 2\alpha_1, \quad v^2 + w^2 = \alpha_2^2.$$

So we have the differential equation that represents and elliptic integral:

$$\dot{w} = (2(\alpha_2 - w)(w + \alpha_2)(w + \alpha_1))^{\frac{1}{2}}$$

The solution to this equation is always periodic [4].

4.4.5 A Few Remarks

The attracting set has a Cantor-like structure. A strange attractor is one defined as having a non-integer dimension. The Lorenz strange attractor has a Hausdorff dimension which is ~ 2.06 [1]. The attractor contains a countable infinity of non-stable periodic orbits and an uncountable infinity of aperiodic orbits and trajectories which terminate at the origin.

An interesting result is that each homoclinic 'explosion' creates a new strange invariant set, and so there will be an uncountable number of topologically distinct attractors in any neighborhood of an arbitrary ρ [5]. I have found no formulas for finding general ρ^* .

5 Numerical Simulations and Figures

For all figures, the parameter will be denoted by an order triplet $\gamma = (\rho, \sigma, \beta)$. Unless otherwise stated, σ , β , will be fixed at $\sigma = 10$, and $\beta = 8/3$. The initial condition will be denoted by \mathbf{x}_0 . As the system has parameters that are of the same order, this is a non-stiff system. For all simulations, MatLab's ODE45 is used with an error tolerance of 1.e-9. The locations of the initial conditions in all figures is given by a black dot. The time interval shown for all figures is $T = [0, 100]$, unless otherwise stated.

5.1 Globally stable , $0 < \rho < 1$

Several tests show global convergence for various parameters with $0 < \rho < 1$, and various initial conditions.

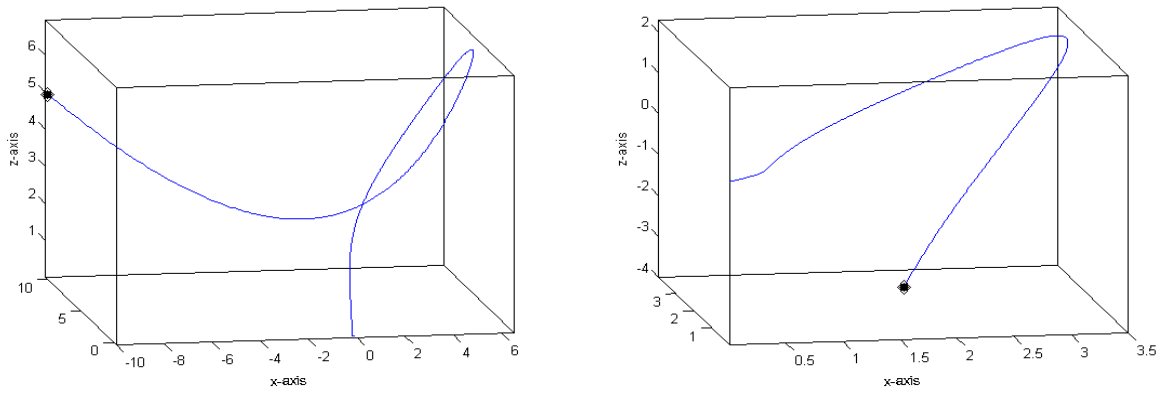


Figure 5.1.1: Stable, $\gamma = (9/10, 10, 8/3)$. LEFT: $\mathbf{x}_0 = (-10, 10, 5)$. RIGHT: $\mathbf{x}_0 = (2, 3, -4)$.

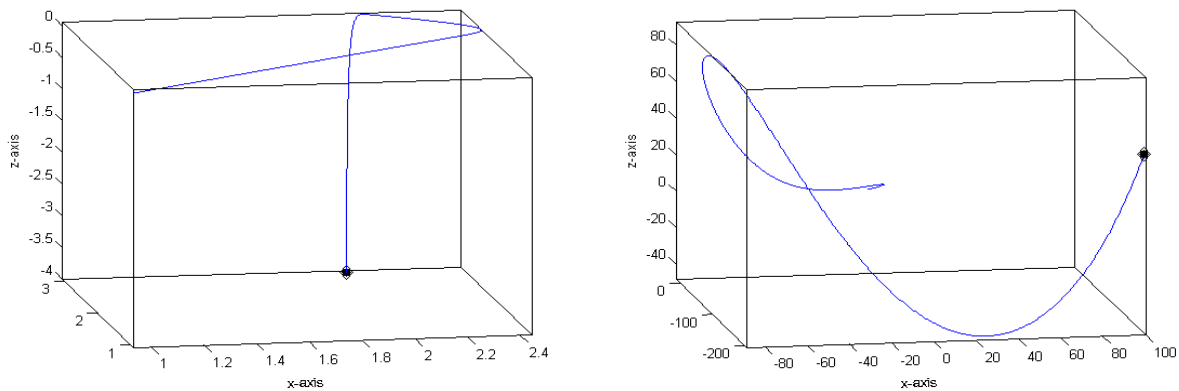


Figure 5.1.2: Stable, LEFT: $\gamma = (9/10, 1, 100)$, $\mathbf{x}_0 = (2, 3, -4)$. RIGHT: $\gamma = (9/10, 30, 100)$, $\mathbf{x}_0 = (100, -200, 50)$.

5.2 Pitchfork Bifurcation, $\rho = 1$

For reference, the origin has a green circle around it. As the z -axis is stable, the initial conditions are taken close. The Bifurcation can be observed as ρ goes from .9 to 1.2. The origin is no longer stable for $\rho > 1$. For Figure 5.2.1, the values for ρ are just under one. Although hard to see, the trajectory of each curve still bends back towards the origin. For Figure 5.2.2, the left figure $\rho = 1.01$, the solution flows towards the y -axis and towards the xy -plane; when it gets on the xy -plane it shoots away from the origin. For the right figure, as the initial data is a small perturbation off of the z -axis, and the z -axis is stable, the trajectory heads towards the origin. As it gets close enough it shoots out towards the equilibrium point q_+ .

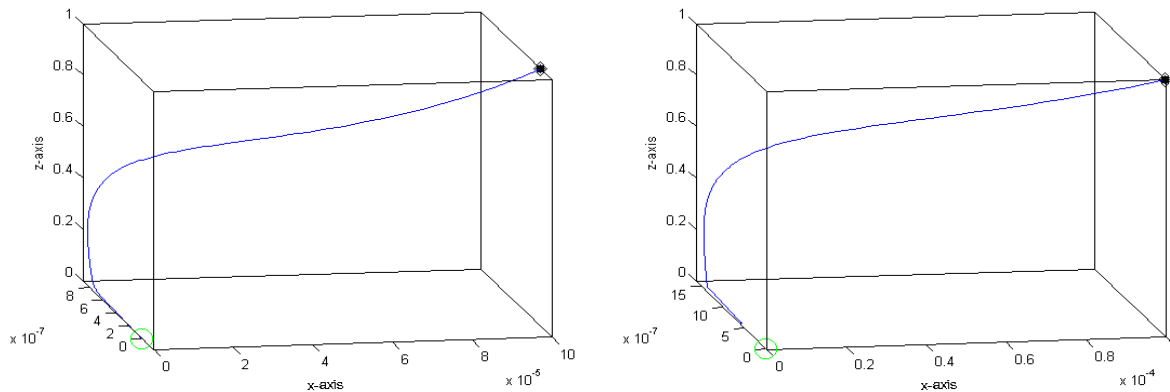


Figure 5.2.1: $\mathbf{x}_0 = (1.e-4, 0, 1)$. LEFT: $\gamma = (9/10, 10, 8/3)$. RIGHT: $\gamma = (99/100, 10, 8/3)$

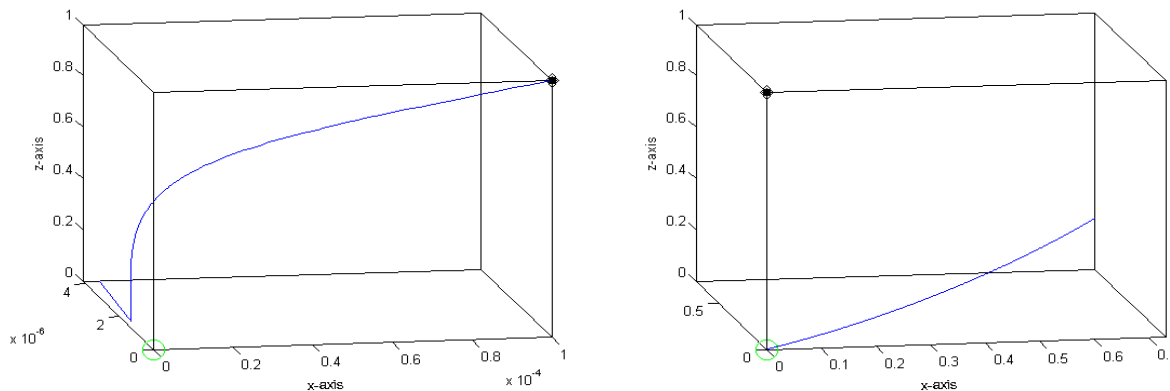


Figure 5.2.2: $\mathbf{x}_0 = (1.e-4, 0, 1)$. LEFT: $\gamma = (1.01, 10, 8/3)$. RIGHT: $\gamma = (1.2, 10, 8/3)$

5.3 Homoclinic orbit

Figures 5.3.1, 5.3.2 illustrate sensitivity to the initial data and to the parameters. $\rho = 13.92655741$ to $\rho + 1.e-9$, completely alters the trajectory. These suggest a homoclinic orbit. In Figure 5.3.3, the right side of the figure shows a trajectory on the stable manifold, The left figure in Figure 5.3.3 shows the trajectory bending around q_- . This is odd behavior, since the analysis shows both fixed points as stable.

5.4 Transient Chaos

Two simulations are run with $\rho = 15$ and $\rho = 24$. For Figure 5.4.1, the initial condition is fixed at $\mathbf{x}_0 = (1, 2, -4)$. As ρ increases from 14 to 24, the transient takes longer to wrap around q_+ , before setting

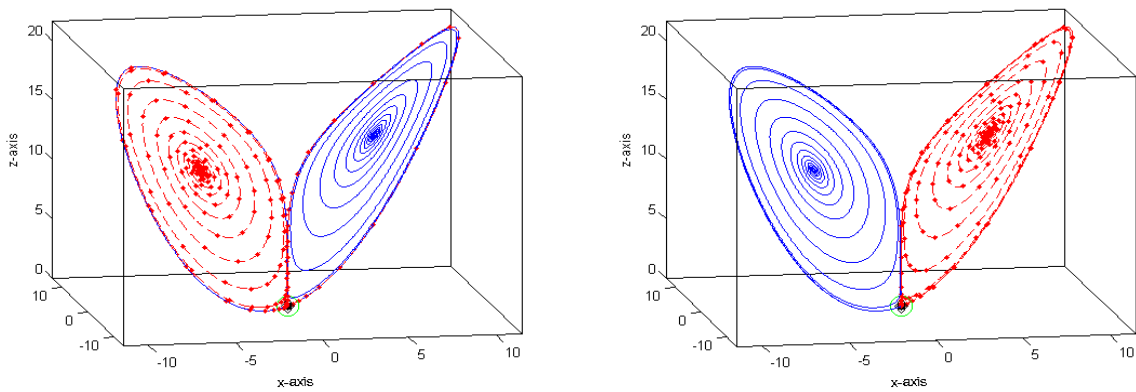


Figure 5.3.1: Red curves with dots: $\mathbf{x}_0=(1.e-16,1.e-16,1.e-16)$, Blue solid curve: $\mathbf{x}_0=(1.e-16,-1.e-16,1.e-16)$. LEFT: $\gamma = (13.92655741, 10, 8/3)$. RIGHT: $\gamma = (13.92655742, 10, 8/3)$.

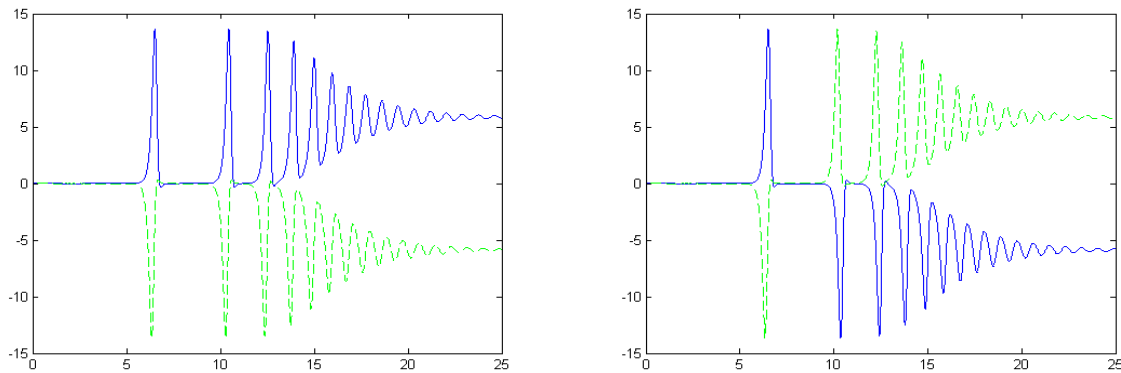


Figure 5.3.2: y-coordinate vs time plots: Green dashed: $\mathbf{x}_0=(1.e-16,-1.e-16,1.e-16)$, Blue solid: $\mathbf{x}_0=(1.e-16,1.e-16,1.e-16)$. LEFT: $\gamma = (13.92655741, 10, 8/3)$. RIGHT: $\gamma = (13.92655742, 10, 8/3)$.

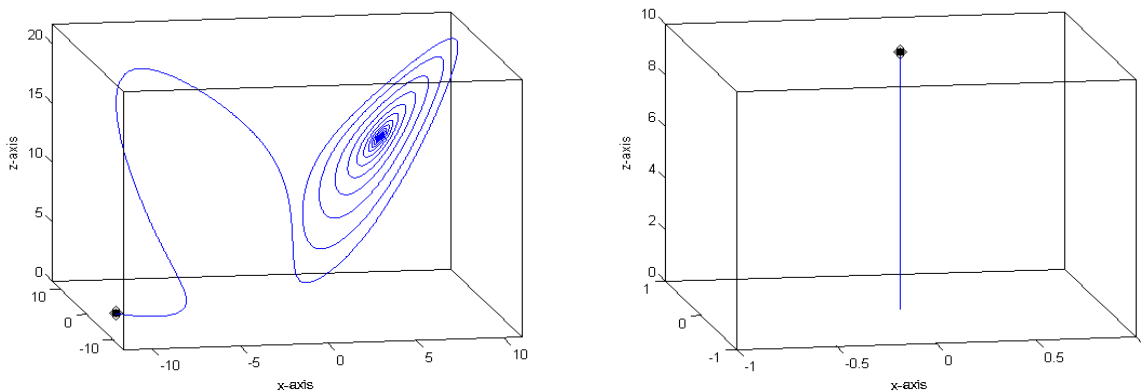


Figure 5.3.3: $\gamma = (13.92655741, 10, 8/3)$. LEFT: $\mathbf{x}_0 = (-10, 0, 0)$. RIGHT: $\mathbf{x}_0 = (0, 0, 10)$.

down into a limit cycle around q_- . For Figure 5.4.2, the initial condition is fixed at $q_+ + 1.e - 5\hat{j}$, where \hat{j} is the unit vector in the y -direction. As ρ increases from 14 to 24, the limit cycle around q_- form larger orbits.

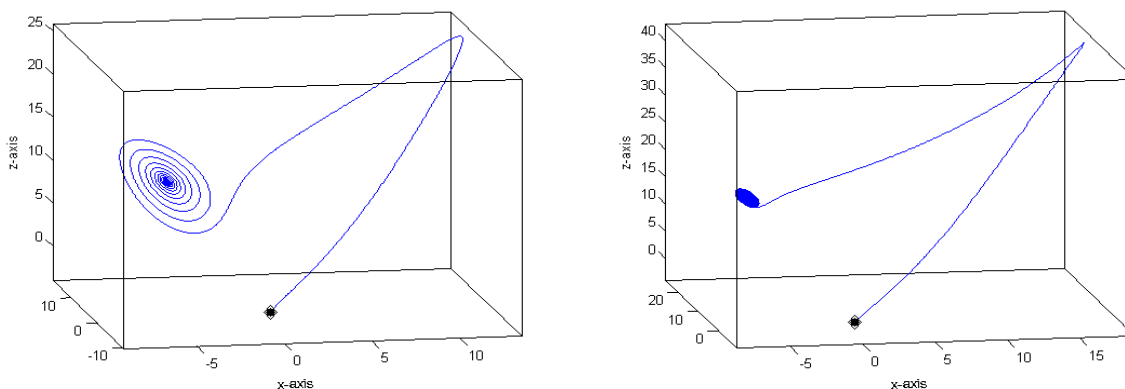


Figure 5.4.1: $\mathbf{x}_0 = (1, 2, -4)$. LEFT: $\gamma = (15, 10, 8/3)$. RIGHT: $\gamma = (24, 10, 8/3)$.

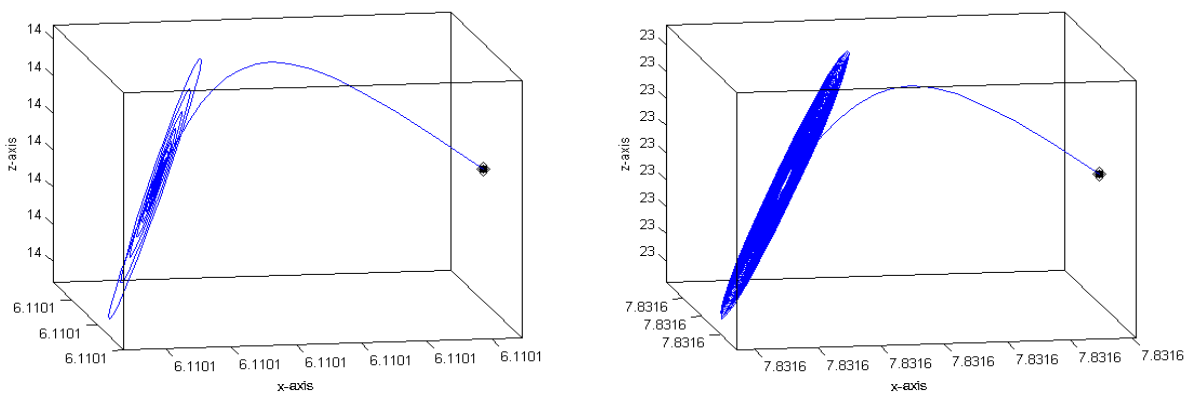


Figure 5.4.2: $q_+ + 1.e - 5\hat{j}$. LEFT: $\gamma = (15, 10, 8/3)$. RIGHT: $\gamma = (24, 10, 8/3)$.

5.5 Chaos

For Figures 5.5.1, 5.5.2, 5.5.3, 5.5.3, $\rho = 28$. Figure 5.5.1 shows typical chaotic behavior. Figure 5.5.2, illustrates a sensitivity to the initial condition. The initial $\mathbf{x}_0 = (1, 2, -4)$ is taken, then perturbed to $\mathbf{x}_0 = (1+1.e-7, 2, -4)$. The trajectories remain close for a time, then start to exhibit chaotic behavior. The plot of the y -coordinate shows this. For Figure 5.5.3 the initial condition is slight perturbation from the fixed point q_+ . The left figure shows $T = [0, 100]$, the right figure shows the trajectory returns to chaotic behavior given a long enough time interval, $T = [0, 200]$. Figure 5.5.4 shows an the trajectory of an initial condition a couple orders of magnitude away from the fixed point. In the left figure $T = [0, 100]$, in the right figure $T = [0, 1]$. This shows the rate of attraction to the attracting set is exponential.

5.5.1 A plot for ρ_h

For Figures 5.5.5, 5.5.6, 5.5.7, $\rho = \rho_h$ with the chosen parameters, $\gamma = (470/19, 10, 8/3)$. The initial condition goes from $\mathbf{x}_0 = (1, 1, -1)$ to $(1, 1, -.95)$. In Figure 5.5.5, we see how a slight change in the initial condition lead to a drastic change in the trajectory. The Right side of 5.5.5 is the x -coordinate versus time. The

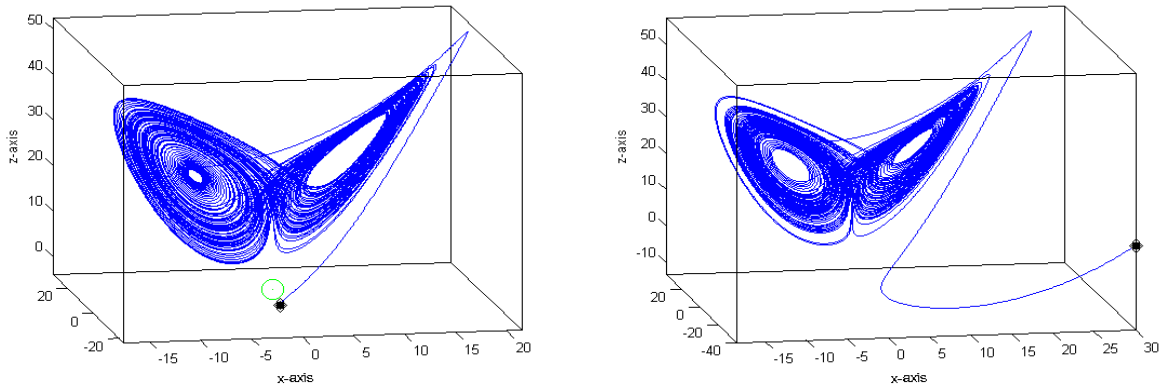


Figure 5.5.1: $\gamma = (28, 10, 8/3)$. LEFT: $\mathbf{x} = (1, 2, -4)$, $\mathbf{x}_0 =$. RIGHT: $\mathbf{x}_0 = (30, -40, 10)$.

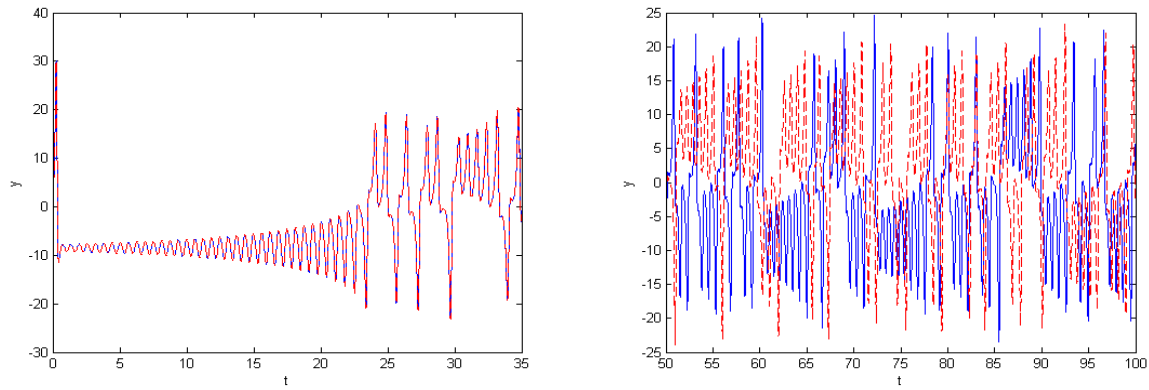


Figure 5.5.2: The Blue curve is $\mathbf{x}_0 = (1, 2, -4)$, The Red dashed curve is $\mathbf{x} = (1 + 1.e-7, 2, -4)$, $\gamma = (28, 10, 8/3)$. LEFT: $T=[0,35]$. RIGHT: $T=[50,100]$.

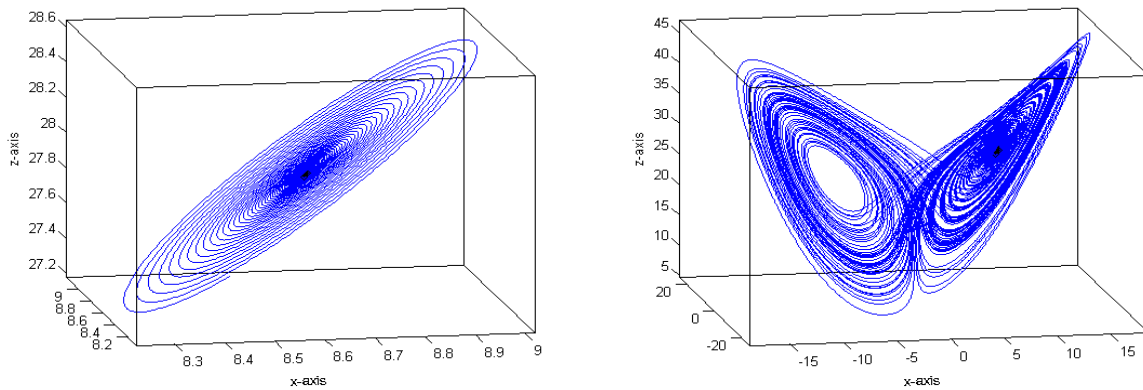


Figure 5.5.3: $\gamma = (28, 10, 8/3)$. $\mathbf{x}_0 = q + 1.e-5\hat{j}$ LEFT: $T = [0, 100]$. RIGHT: $T = [0, 200]$.

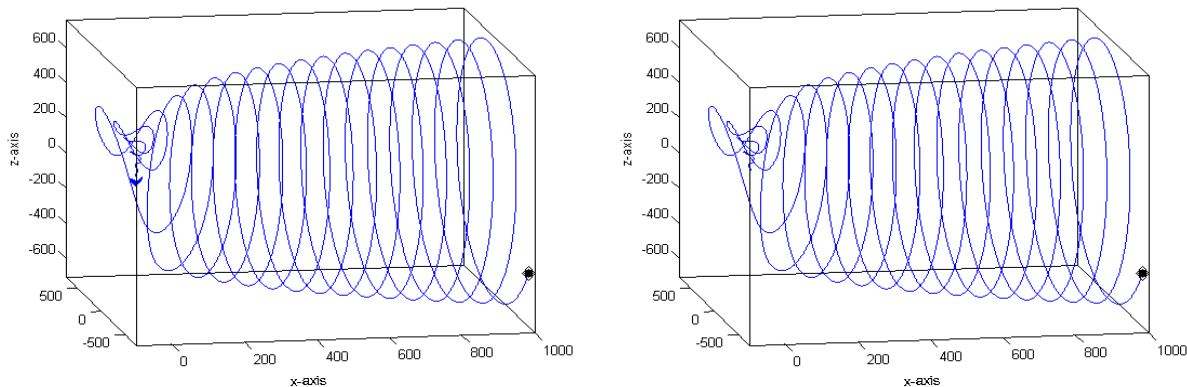


Figure 5.5.4: $\gamma = (28, 10, 8/3)$. $\mathbf{x}_0 = (1000, -600, -400)$ LEFT: $T = [0, 100]$. RIGHT: $T = [0, 1]$.

trajectory is nearly stable until about $t = 40$. Figure 5.5.6, is a closer look at the trajectory of the y -coordinate. The left figure shows time $T = [0, 35]$, which is stable. The right figure is from $t = [50, 100]$, this is chaotic behavior. Figure 5.5.7 shows the z -coordinate, this remains stable with the perturbation.

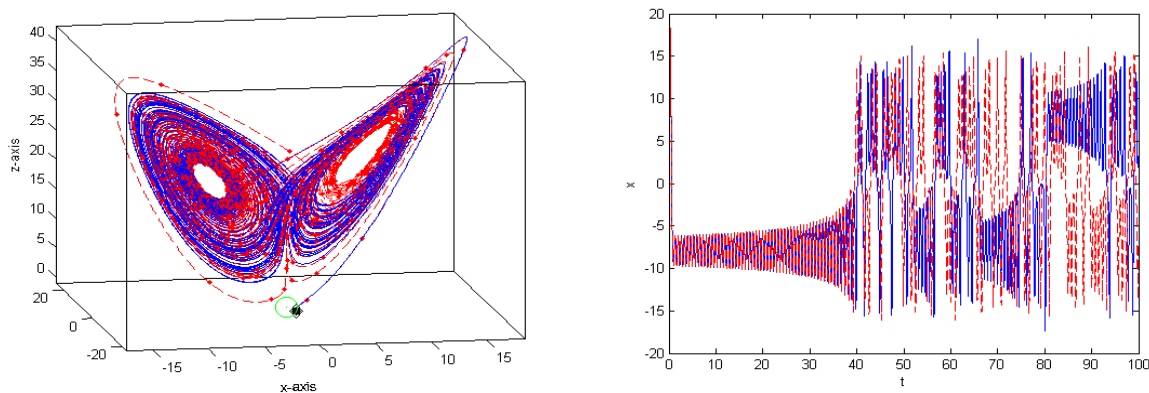


Figure 5.5.5: Blue curve $\mathbf{x}_0 = (1, 1, -1)$, Red dotted curve $\mathbf{x}_0 = (1, 1, -.95)$. LEFT: $T = [0, 25]$. RIGHT: $T = [50, 100]$.

5.6 Other Notable Orbits

For values of $\rho > \rho_h$, the system exhibits an array of different behavior. In the following subsections, several values of ρ are chosen to illustrate this the various behaviors.

5.6.1 Double Periodic Orbits

When $\rho = 144$, the solution show a double periodic orbit. Two different initial conditions are chosen, with small perturbation for each. In all cases the solution converges to this double periodic orbit. For Figure 5.6.1, the initial conditions are taken to be $\mathbf{x}_0 = q_+ + \epsilon \hat{j}$, $q_+ - \epsilon \hat{j}$, where $\epsilon = 1.e - 8$, and \hat{j} is the unit vector in the y -direction. For Figure 5.6.2, the initial conditions are, $\mathbf{x}_0 = (1, 1, -1)$, $(1, 1, -.95)$. For this example, the small perturbation does not affect the trajectory of the solution.

5.6.2 Intermittent Chaos

For $\rho = 167$, two solutions starting near each other phase in and out of sync. The solution almost go into a double periodic orbit, then to a chaotic orbit. This pattern repeats indefinitely. Figure 5.6.3, shows this

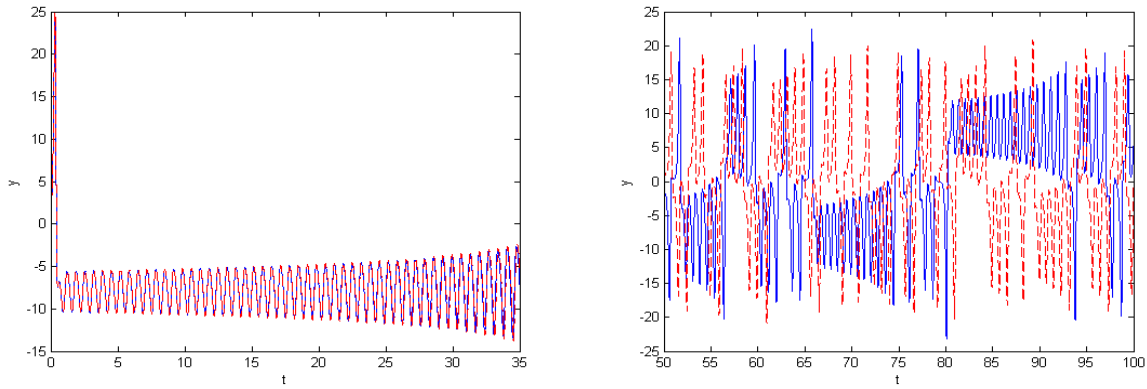


Figure 5.5.6: Y-coordinate plot: Blue curve $\mathbf{x}_0 = (1, 1, -1)$, Red dashed curve $\mathbf{x}_0 = (1, 1, -0.95)$. LEFT: $T = [0, 25]$. RIGHT: $T = [50, 100]$.

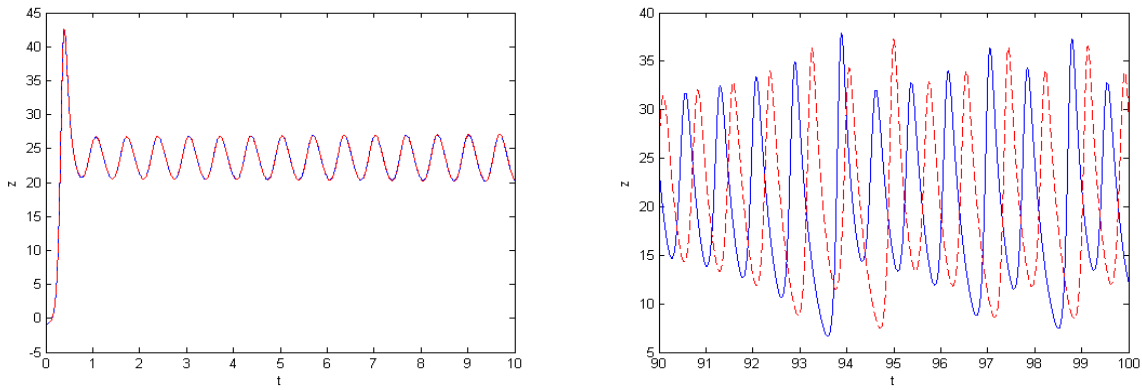


Figure 5.5.7: Z-coordinate plot: Blue curve $\mathbf{x}_0 = (1, 1, -1)$, Red dashed curve $\mathbf{x}_0 = (1, 1, -0.95)$. LEFT: $T = [0, 10]$. RIGHT: $T = [90, 100]$.

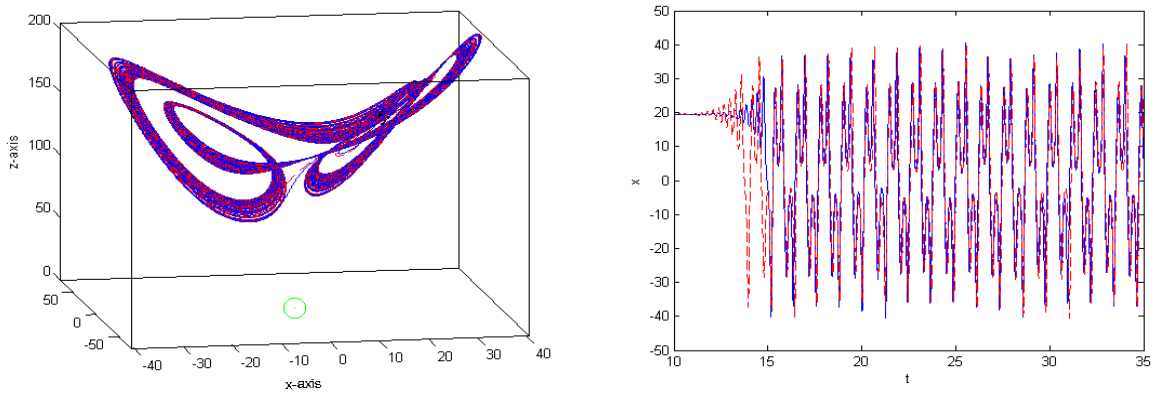


Figure 5.6.1: Blue curve $\mathbf{x}_0 = q_+ + \epsilon \hat{j}$, Red dashed curve $\mathbf{x}_0 = q_+ - \epsilon \hat{j}$. LEFT: Solution plot. RIGHT: x -coordinate plot for $T = [10, 35]$.

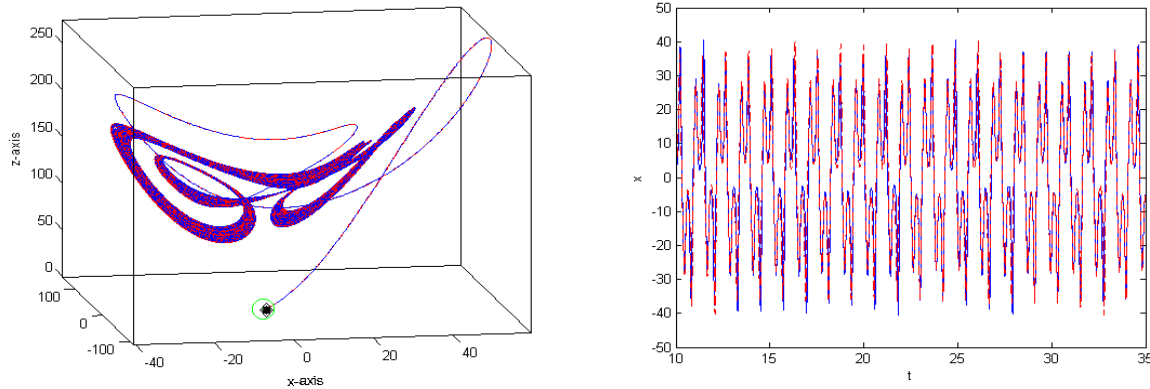


Figure 5.6.2: Blue curve $\mathbf{x}_0 = (1, 1, -1)$, Red dashed curve $\mathbf{x}_0 = (1, 1, -.95)$. LEFT: Solution plot. RIGHT: $T = [10, 35]$.

near chaos like behavior. The right side of Figure 5.6.3, shows the z -coordinate going in sync, then out of sync. Figure 5.6.4 shows the same behavior for the y -coordinate and x -coordinate plots.

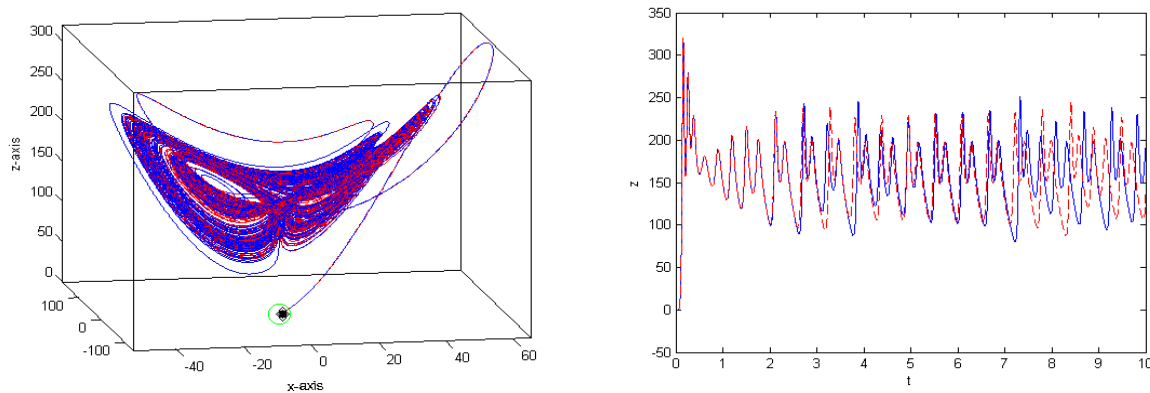


Figure 5.6.3: Blue curve $\mathbf{x}_0 = (1, 1, -1)$, Red dashed curve $\mathbf{x}_0 = (1, 1, -.95)$. LEFT: Solution plot. RIGHT: z -coordinate plot for $T = [0, 10]$.

5.6.3 A Periodic Orbit

For $\rho = 400$, the phase space shows a periodic orbit. Two initial conditions are shown, $\mathbf{x} = (1, 1, 1)$ and $q_+ - \epsilon \hat{j}$, where $\epsilon = 1.e-8$. In Figure 5.6.5, the left figure shows both solutions approaching the same orbit. The right figure in Figure 5.3.1, shows the x -coordinate plot for $T = [10, 35]$, both solutions are nearly identical. Figure 5.6.6 shows the y, z -coordinate plots. In the left figure, after a $t > 10$, the period becomes identical. The same behavior is observed in the right plot for the z -coordinate. The solution starting near the fixed point matches the orbit after about $t = 10$.

6 MATLAB Code

6.1 LORENZ.m:

```
% Computes the solution to the Lorenz system given prescribed initial
% conditons and parameters using MATLAB's ODE45.
%
```

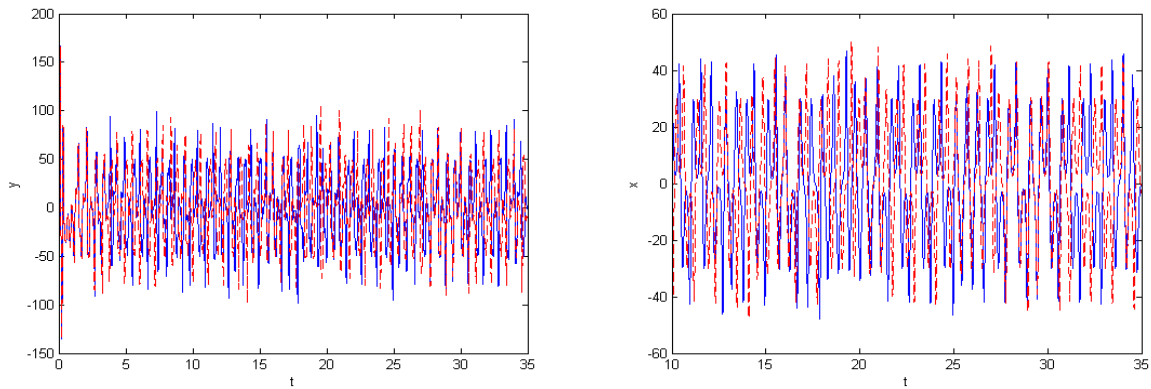


Figure 5.6.4: Blue curve $\mathbf{x}_0 = (1, 1, -1)$, Red dashed curve $\mathbf{x}_0 = (1, 1, -0.95)$. LEFT: y -coordinate plot for $T = [0, 35]$ RIGHT: x -coordinate plot for $T = [10, 35]$.

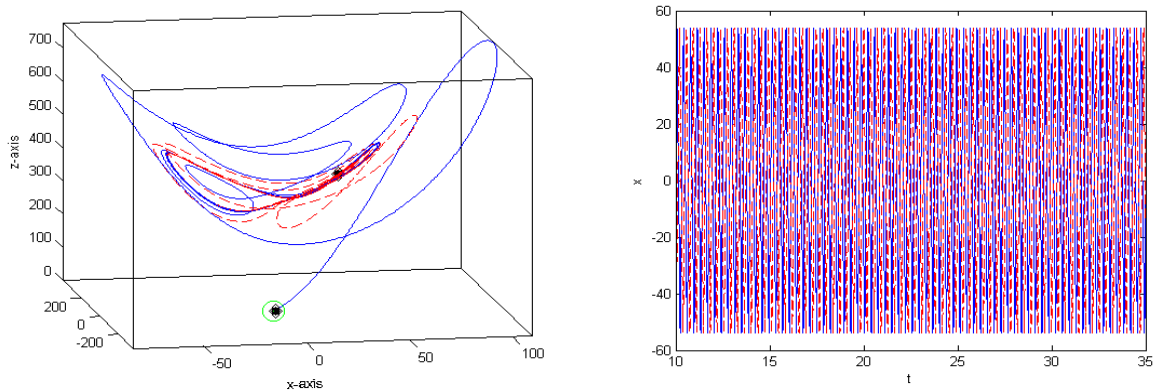


Figure 5.6.5: Blue curve $\mathbf{x}_0 = (1, 1, 1)$, Red dashed curve $q_+ - \epsilon \hat{j}$. LEFT: Solution plot. RIGHT: x -coordinate plot for $T = [10, 35]$.

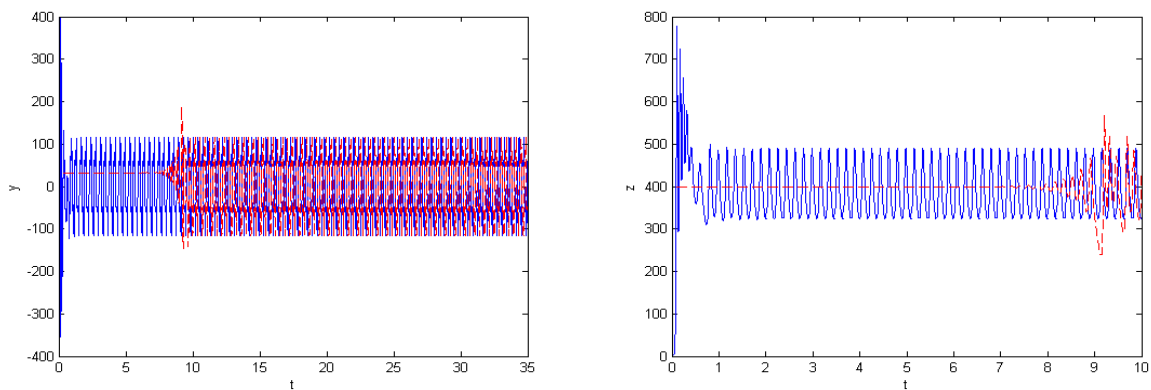


Figure 5.6.6: Blue curve $\mathbf{x}_0 = (1, 1, 1)$, Red dashed curve $q_+ - \epsilon \hat{j}$. y -coordinate plot for $T = [10, 35]$ RIGHT: z -coordinate plot for $T = [0, 10]$.

```

% INPUT:
%     RHO     - Scaled Rayleigh number.
%     SIGMA   - Prandtl number.
%     BETA    - Geometry aspect ratio.
%     INI     - Initial point.
%     T       - Time interval T = [ta,tb]
%     EPS     - ode45 solver precision
%
% OUTPUT:
%     x       - x-coordinate of solution.
%     y       - y-coordinate of solution.
%     z       - z-coordinate of solution.
%     t       - Time interval for [x(t),y(t),z(t)]
%

```

Initializations

```

if nargin<4
    eps = 1.e-9;
    T = [0 100];
    ini = [1 1 1];
end

if nargin < 5
    T = [0 100];
    ini = [1 1 1];
end

if nargin < 6
    ini = [1 1 1];
end
options = odeset('RelTol',eps,'AbsTol',[eps eps eps/10]);

```

Solve system

```
[t,X] = ode45(@(T,X) sys(X, sigma, rho, beta), T, ini, options);
```

Set output

```
x = X(:,1); y = X(:,2); z = X(:,3);
```

6.2 LORENZ_SYS.M

```

function dx = lorenz_sys(X, sigma, rho, beta)

% Computes the vector field for the Lorenz system:
%     x' = sigma*(y-x)
%     y' = x*(rho - z) - y
%     z' = x*y - beta*z
% INPUT:
%     RHO     - Scaled Rayleigh number.
%     SIGMA   - Prandtl number.
%     BETA    - Geometry aspect ratio.
% OUTPUT:
%     dx      - Vector field for Lorenz system.

```

System

```

dx = zeros(3,1);
dx(1) = sigma*(X(2) - X(1));
dx(2) = X(1)*(rho - X(3)) - X(2);
dx(3) = X(1)*X(2) - beta*X(3);

```

6.3 LORENZ_SYS_VEC.M

```

function dx = lorenz_sys_vec(x,y,z, sigma, rho, beta)

% Computes the vector field for the Lorenz system for vector input.
%      x' = sigma*(y-x)
%      y' = x*(rho - z) - y
%      z' = x*y - beta*z
% INPUT:
%   RHO      - Scaled Rayleigh number.
%   SIGMA    - Prandtl number.
%   BETA     - Geometry aspect ratio.
% OUTPUT:
%   dx       - Vector field for Lorenz system.

```

System

```

dx = zeros(3,length(x));
dx(1,:) = sigma*(y - x);
dx(2,:) = x.*(rho - z) - y;
dx(3,:) = x.*y - beta*z;

```

6.4 PLOTTING_SCRIPT.M**Set parameters**

```

close all; clear all; clc;

% Test parameters for rho with sigma = 10, beta = 8/3;
%      rho < 1;           %Stable Trajectories
%      rho = 1;          %Pitchfork Bifurcation near origin
%      rho = 13.92655741; %Homoclinic orbit near origin
%      rho = 13.92655742; %Homoclinic orbit near origin
%      rho = 28;         %Chaos
%      rho = sigma*(sigma + beta + 3)/(sigma-beta-1);%Hopf bifurcation
%
%Use rho, for solution with a single initial conditons.
%Use rho1,rho2 to compare two initial conditions
%rho1 = 40;
%rho2 = rho1;
rho = 100;
sigma = 10;
beta = 8/3;

```

Various initial conditions

```

%p = [1.e-16,1.e-16,1.e-16]; %Pertubation of origin
%p = [1.e-16,-1.e-16,1.e-16]; %Pertubation of origin
%p = [sqrt(beta*(rho - 1)),sqrt(beta*(rho - 1)),rho - 1];% fixed point

```

```

%p = [sqrt(beta*(rho - 1))-1.e-8,sqrt(beta*(rho - 1)),rho - 1];
%
%                               Pertubation of fixed point
%
%p1 = [1,1,-1];
%p2 = [1,1,-.95];
p = [1,1,1];

```

Set Solver options and plot options

```

T = [0 100];           %Time interval for solution T = [ta,tb];
eps = 1.e-9;          %Persicion for ode45
plot_data = 0;        %0 = Single initial condition
                        %1 = Two phase portaits together
                        %2 = Two phase portaits seperately

```

```

if plot_data == 0
    [X,Y,Z,t] = lorenz(rho, sigma, beta, p, T, eps);
else
    [X1,Y1,Z1,t1] = lorenz(rho1, sigma, beta, p1, T, eps);
    [X2,Y2,Z2,t2] = lorenz(rho2, sigma, beta, p2, T, eps);
end

```

Plot

```

if plot_data == 1
    M = floor(sqrt(length(t1))/2);
    figure
    plot3(X1,Y1,Z1,'--r');
    hold on
    plot3(X1(1:M:end),Y1(1:M:end),Z1(1:M:end),'r','Marker','.', 'linestyle', 'none');
    plot3(p1(1),p1(2),p1(3),'MarkerSize',20,'Marker','.', 'color', 'k');
    plot3(p1(1),p1(2),p1(3),'MarkerSize',10,'Marker','d', 'color', 'k');
    plot3(0,0,0,'MarkerSize',15,'Marker','o', 'color', 'g');
    axis tight;
    box on
    xlabel('x-axis');
    ylabel('z-axis');
    view([-10 15])
    xlab = get(gca,'xlabel');
    set(xlab,'rotation',3)
    %
    figure
    plot3(X2,Y2,Z2);
    hold on
    plot3(p2(1),p2(2),p2(3),'MarkerSize',20,'Marker','.', 'color', 'k');
    plot3(p2(1),p2(2),p2(3),'MarkerSize',10,'Marker','d', 'color', 'k');
    plot3(0,0,0,'MarkerSize',15,'Marker','o', 'color', 'g');
    axis tight;
    box on
    xlabel('x-axis');
    ylabel('z-axis');
    view([-10 15])
    xlab = get(gca,'xlabel');
    set(xlab,'rotation',3)
elseif plot_data == 2

```

```

    figure
    plot3(X1,Y1,Z1);
hold on
    plot3(X2,Y2,Z2,'--r');
    plot3(p1(1),p1(2),p1(3),'MarkerSize',20,'Marker','.', 'color', 'k');
    plot3(p1(1),p1(2),p1(3),'MarkerSize',10,'Marker','d', 'color', 'k');
    plot3(p2(1),p2(2),p2(3),'MarkerSize',20,'Marker','.', 'color', 'k');
    plot3(p2(1),p2(2),p2(3),'MarkerSize',10,'Marker','d', 'color', 'k');
    plot3(0,0,0,'MarkerSize',15,'Marker','o', 'color', 'g');
    axis tight;
    box on
    xlabel('x-axis');
    zlabel('z-axis');
    view([-10 15])
    xlab = get(gca,'xlabel');
    set(xlab,'rotation',3)
else
    M = floor(sqrt(length(t))/2);
    figure
    plot3(X,Y,Z);
    hold on
    plot3(p(1),p(2),p(3),'MarkerSize',20,'Marker','.', 'color', 'k');
    plot3(p(1),p(2),p(3),'MarkerSize',10,'Marker','d', 'color', 'k');
    plot3(0,0,0,'MarkerSize',15,'Marker','o', 'color', 'g');
    axis tight;
    box on
    xlabel('x-axis');
    zlabel('z-axis');
    view([-10 15])
    xlab = get(gca,'xlabel');
    set(xlab,'rotation',3)
end

if plot_data == 1 || plot_data == 2

```

X Plots

```

    figure
    plot(t1,X1);
    hold on
    plot(t2,X2,'--r');
    hold off
    xlabel('t')
    ylabel('x')
%
    figure
    K1 = find(t1 >50);
    plot(t1(K1),X1(K1));
    hold on
    K2 = find(t2 >50);
    plot(t2(K2),X2(K2),'--r');
    hold off
    xlabel('t')
    ylabel('x')
%
```

```
figure
L1 = find(t1 < 35);
plot(t1(L1),X1(L1));
hold on
L2 = find(t2 < 35);
plot(t2(L2),X2(L2),'--r');
hold off
xlabel('t')
ylabel('x')
```

Y plots

```
figure
K1 = find(t1 >50);
plot(t1(K1),Y1(K1));
hold on
K2 = find(t2 >50);
plot(t2(K2),Y2(K2),'--r');
hold off
xlabel('t')
ylabel('y')
```

%

```
figure
L1 = find(t1 < 35);
plot(t1(L1),Y1(L1));
hold on
L2 = find(t2 < 35);
plot(t2(L2),Y2(L2),'--r');
hold off
xlabel('t')
ylabel('y')
```

Z-plots

```
figure
K1 = find(t1 >90);
plot(t1(K1),Z1(K1));
hold on
K2 = find(t2 >90);
plot(t2(K2),Z2(K2),'--r');
hold off
xlabel('t')
ylabel('z')
```

%

```
figure
L1 = find(t1 < 10);
plot(t1(L1),Z1(L1));
hold on
L2 = find(t2 < 10);
plot(t2(L2),Z2(L2),'--r');
hold off
xlabel('t')
ylabel('z')
```

end

Bibliography

- [1] P. Grassberger and I. Procaccia. Measuring the strangeness of strange attractors. *Physica D: Nonlinear Phenomena*, 9(12):189 – 208, 1983.
- [2] B. Hassard and J. Zhang. Existence of a homoclinic orbit of the lorenz system by precise shooting. *SIAM Journal on Mathematical Analysis*, 25(1):179–196, 1994.
- [3] S. Hastings and W. Troy. A proof that the lorenz equations have a homoclinic orbit. *Journal of Differential Equations*, 113(1):166 – 188, 1994.
- [4] C. Sparrow. *The Lorenz Equations: Bifurcations, Chaos, and Strange Attractors*. Applied Mathematical Sciences. Springer New York, 1982.
- [5] R. Williams. The structure of lorenz attractors. *Publications Mathématiques de l'Institut des Hautes études Scientifiques*, 50(1):73–99, 1979.
- [6] J. Yorke and E. Yorke. Metastable chaos: The transition to sustained chaotic behavior in the lorenz model. *Journal of Statistical Physics*, 21(3):263–277, 1979.